

# Supervised Segmentation of Very High Resolution Images by the Use of Extended Morphological Attribute Profiles and a Sparse Transform

Jiayi Li, *Student Member, IEEE*, Hongyan Zhang, *Member, IEEE*, and Liangpei Zhang, *Senior Member, IEEE*

**Abstract**—In this letter, a novel supervised segmentation technique based on sparsely representing the stacked extended morphological attribute profiles (EAPs) and maximum *a posteriori* probability (MAP) is presented for very high resolution (VHR) images. Attribute profiles (APs), which are extracted by using several attributes, are applied to the multispectral VHR image, leading to a set of extended EAPs. Using the sparse prior of representing the pixel with all training samples, the extended multi-AP (EMAP) feature stacked by the EAP features is transformed into a class-dependent residual feature, which can be normalized as a posterior probability distribution of the pixel. A graph-cut approach is utilized to segment the image scene and obtain the final classification result. Experiments were conducted on IKONOS and WorldView-2 data sets. Compared with SVM, object-oriented SVM with majority voting, and some other state-of-the-art methods, the proposed method shows stable and effective results.

**Index Terms**—Extended attribute profile (EAP), graph cut, segmentation, sparse representation, very high resolution (VHR) images.

## I. INTRODUCTION

IN RECENT years, the latest generation of optical sensors with very high resolution (VHR) has broadened the range of remote sensing applications. Exploring the abundant information of the VHR images to address the analysis problem of land-cover/use and urban mapping is an active area of research. Although the increased geometrical resolution detailing the surveyed scene leads to a fine representation, VHR image analysis still faces some obstacles. The first problem comes as a result of the significantly increased complexity of the images in the spatial domain, which aggravates the spectral differences of the same land-cover type. The second challenge is that the decreased resolution in the spectral domain increases the spectral ambiguity of the different land-cover types.

In order to deal with such problems and derive a spatially accurate labeling map, it is advisable to utilize geometrical features in the analysis process. To effectively describe the geo-

Manuscript received September 28, 2013; revised November 1, 2013; accepted December 4, 2013. Date of publication January 10, 2014; date of current version March 11, 2014. This work was supported in part by the National Basic Research Program of China (973 Program) under Grant 2011CB707105, by the National Natural Science Foundation of China under Grant 61201342 and Grant 40930532, and by the Program for Changjiang Scholars and Innovative Research Team in University under Grant IRT1278.

The authors are with the State Key Laboratory of Information Engineering in Surveying, Mapping, and Remote Sensing, Wuhan University, 430079 Wuhan, China (e-mail: zhanghongyan@whu.edu.cn).

Color versions of one or more of the figures in this paper are available online at <http://ieeexplore.ieee.org>.

Digital Object Identifier 10.1109/LGRS.2013.2294241

metrical information of a VHR image, morphological attribute profiles (APs), which provide a multilevel characterization of an image, can be used to model the different kinds of structural information [1]. In [2], the extended AP (EAP), combining the APs from different attributes, was presented to highlight the discrimination of different remote sensing pixels and achieve a desirable classification result.

Sparsity of signals, denoting that most natural signals can be compactly represented by only a few coefficients in a certain basis or dictionary, with almost no performance loss [3], [4], has been widely used in many image processing and analysis applications [5], [6]. For supervised classification, the best-known algorithm, i.e., sparse representation classification (SRC) [5], stacks all the training samples as the overcomplete dictionary, assuming that only the coefficients associated with the underlying training samples are nonzero, and obtains state-of-the-art performance. Applying this method to hyperspectral image classification, Chen *et al.* [7] imposed contextual information to the sparse representation model by stacking the contextual signals of the test pixel, and further research based on [7] can be found in [8] and [9], which achieved an improved classification result.

In spite of the rising research interest in sparse representation for hyperspectral imagery, there have been very few studies that have considered VHR imagery. In this letter, we utilize an SRC-based transform for the VHR image and the Bayesian approach to segmentation. The algorithm is implemented in the following three steps: 1) feature construction, which concatenates all the EAPs in a single vector of features to preserve the geometrical information of the original image scene; 2) a sparse transform, where the posterior probability distributions are modeled by a sparse representation approach based on SRC; and 3) segmentation, which utilizes the posterior probability distributions and the multilevel logistic prior to derive the class labels of all the image pixels. The final result of the proposed method is obtained by a maximum *a posteriori* (MAP) segmentation process, which is computed via an efficient min-cut-based integer optimization method [10], [11]. The main novelty of the proposed method, which exhibits good discriminatory capability when dealing with this ill-posed problem, is the integration of the posterior probability distributions, which are extracted by sparsely representing the EMAP feature and the Bayesian segmentation. Experiments on two VHR images confirm the effectiveness of the proposed algorithm.

The remainder of this letter is organized as follows: Section II introduces the proposed algorithm. Section III evaluates the

effectiveness of the proposed method via experiments with IKONOS and WorldView-2 data sets. Section IV concludes this letter.

## II. PROPOSED APPROACH

### A. EMAP Feature Extraction

The extended multi-AP (EMAP) feature, which is constructed by combining each EAP in the respective attributes in a single vector of features, can preserve the geometrical information as well as the spectral information. The EAP feature proposed in [1] is a generalization of the widely used MPs [12] and is generated by concatenating many APs. Considering a multispectral image with  $c$  bands, the EAP can be denoted as

$$EAP = \{AP(B_1), AP(B_2), \dots, AP(B_k) \dots, AP(B_c)\} \quad (1)$$

where  $B_k$  refers to the  $k$ th band of the VHR image ( $k = 1, \dots, c$ ). According to criterion  $T$  with  $n$  morphological attribute thickening ( $\phi^T$ ) operators and  $n$  morphological attribute thinning ( $\gamma^T$ ) operators, the AP is obtained by the morphological filter by reconstruction and can be shown as

$$AP(B_k) = \left\{ \phi_n^T(B_k), \phi_{n-1}^T(B_k), \dots, \phi_1^T(B_k) \right. \\ \left. B_k, \gamma_1^T(B_k), \dots, \gamma_{n-1}^T(B_k), \gamma_n^T(B_k) \right\} \quad (2)$$

where the given criterion  $T$  associated with the transformation is evaluated on each connected component of the image. APs are connected operators, which operate on the connected components that compose an image [13]. In general, the criterion compares the value of an arbitrary attribute *attr* (e.g., area, volume, and standard deviation) measured on component  $C$  against a given reference filter parameter value  $\lambda$ . For the thickening transformation, the regions will be set to the gray level of a darker surrounding region if the criterion is verified; for the thinning transformation, the processing will be set to the contrary.

It has been suggested that attribute filters can be efficiently computed by taking advantage of the representation of the input image as a rooted hierarchical tree of the connected components of the image [2]. In this letter, we utilize the area, standard deviation, diagonal box, and the moment of inertia as meaningful attributes to construct the EMAP feature for the VHR image, as suggested in [1] and [14]. The Profatran software, which was kindly provided by the author in [15], is utilized to calculate the EAP features in this letter.

### B. Posterior Probability Distribution via a Sparse Transform

Since it is believed that the EMAP feature can effectively consider both the geometrical information and the spectral information, we replace the original spectral feature with the EMAP feature for the following posterior probability distribution estimation. For a VHR scene, we denote  $\mathbf{y} \in \mathcal{L}^o$  as the image of the labels,  $\mathcal{M} = \{1, \dots, M\}$  as the set of  $M$  classes, and  $\mathbf{S} = [s_1, \dots, s_j, \dots, s_o] \in \mathbb{R}^{E \times o}$  (where  $E$  refers to the number of the dimensionality of the EMAP feature, and  $o$  refers to the number of pixels in the scene,  $j = 1, \dots, o$ ). In the sparse representation model, we stack the given  $N_i$  ( $i = 1, \dots, M$ )

training pixels from the  $i$ th class as columns of a dictionary  $\mathbf{A}_i = [\mathbf{a}_{i,1}, \mathbf{a}_{i,2}, \dots, \mathbf{a}_{i,N_i}] \in \mathbb{R}^{E \times N_i}$ ; then, the overcomplete dictionary  $\mathbf{A} = \mathbb{R}^{E \times N}$  with  $N = \sum_{i=1}^M N_i$  is constructed by combining all the subdictionaries  $\{\mathbf{A}_i\}_{i=1, \dots, M}$  [16]. This way, the pixel  $s_j$  that belongs to the  $i$ th class can be sparsely represented as a linear combination of all the given training samples, i.e.,

$$s_j = \mathbf{A}_1 \beta_1 + \dots + \mathbf{A}_i \beta_i + \dots + \mathbf{A}_M \beta_M + \xi_j \\ = \underbrace{[\mathbf{A}_1 \dots \mathbf{A}_i \dots \mathbf{A}_M]}_{\mathbf{A}} \underbrace{[\beta_1 \dots \beta_i \dots \beta_M]^T}_{\boldsymbol{\beta}} + \xi_j \quad (3)$$

where  $\boldsymbol{\beta}$  is a sparse coefficient vector, in which only the entries of  $\beta_i$  are assumed to be nonzero, and  $\xi_j$  is the random noise. The coefficient vector  $\boldsymbol{\beta}$  can be obtained by solving the following optimization problem:

$$\boldsymbol{\beta} = \arg \min \|A\boldsymbol{\beta} - s\|_2^2 \quad \text{s.t.} \quad \|\boldsymbol{\beta}\|_0 \leq N_i. \quad (4)$$

It is clear that these aforementioned problems are NP-hard. In general, there are two effective ways of solving such a problem: the greedy-pursuit-based algorithms [17] and the  $\ell_1$ -norm convex relaxation algorithms [18].

After obtaining the sparse coefficient vector  $\boldsymbol{\beta}$ , the posterior probability can be defined with respect to the residuals associated with each label. For each class  $i$ , set  $\delta_i: \mathbb{R}^N \rightarrow \mathbb{R}^N$  to be the characteristic function that selects the coefficients associated with the  $i$ th class. For  $\boldsymbol{\beta} \in \mathbb{R}^N$ ,  $\delta_i(\boldsymbol{\beta}) \in \mathbb{R}^N$  is a new vector whose only nonzero entries are the ones in  $\boldsymbol{\beta}$  that are associated with class  $i$ . With the residual for each class  $r_{i,j} = \|\mathbf{s}_j - \mathbf{A}\delta_i(\boldsymbol{\beta})\|_2$ , it is believed that the pixel will be classified to the label with the least residual in the well-known SRC. In other words, the label with the least residual has the most probability to be labeled than other classes, as the principle of the maximum posterior probability. It is likely to point out that the posterior probability  $p(y_{i,j}|s_j)$  is inversely proportional to  $r_{i,j}$ , i.e.,

$$p(y_{i,j}|s_j) = \frac{1}{r_{i,j}\chi} \quad (5)$$

where  $y_{i,j}$  refers to labeled class  $i$  for the pixel  $s_j$ , and  $\chi = 1/\sum_{k=1}^M r_{k,j}$  is a normalized constant.

### C. MLL Prior and MAP Segmentation

The segmentation method used in this letter is MAP segmentation [11]. In the Bayesian framework, the labeling processing is usually conducted by maximizing the posterior distribution as follows:

$$p(\mathbf{y}|s) \propto p(s|\mathbf{y})p(\mathbf{y}). \quad (6)$$

Assuming conditional independence of the EMAP feature, given the label and the equal probability for each class, the proposed algorithm for a VHR image based on MAP segmentation can be denoted as

$$\mathbf{y} = \arg \max_{\mathbf{y} \in \mathcal{L}^o} \left\{ \sum_{j=1}^o \log p(y_j|s_j) + \log p(\mathbf{y}) \right\} \quad (7)$$

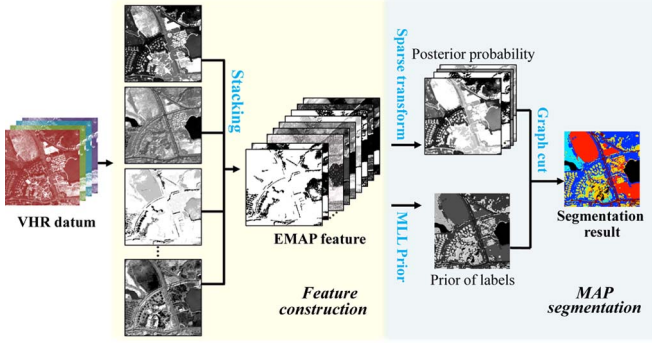


Fig. 1. Block diagram summarizing the most relevant steps of the proposed method.

TABLE I  
CLASSIFIERS UTILIZED IN THE EXPERIMENT SECTION

Name	Feature	Processing level
SRC	S	PC
SVM	S	PC
SRC_EAP	E	PC
SVM_EAP	E	PC
OOSRC	S	OOC
OOSVM	S	OOC
OOSRC_EAP	E	OOC
OOSVM_EAP	E	OOC
Proposed	E	Seg

where  $y_j$  refers to label  $j$  for the image.

To deal with this segmentation problem, of which the first one can be calculated by sparse transforms (5) and (6), we now utilize a multilevel logistic (MLL) approach [19] to model the second term of (7). This MLL approach, which exploits the fact that spatially neighboring pixels are likely to belong to the same class, has been widely used in image segmentation. Due to space limitations,  $p(\mathbf{y})$  can be succinctly shown as

$$p(\mathbf{y}) = \frac{1}{Z} e^{-\mu \sum_{(m,n) \in \mathcal{C}} \varphi(y_m - y_n)} \quad (8)$$

where  $\mathcal{C}$  denotes a neighboring patch of the image,  $\varphi(y)$  denotes the unit impulse function, and  $\mu$  controls the level of smoothness of the segmentation map. (For more details of the MLL prior, please refer to [11] and [19].)

Based on the aforementioned approach, the MAP segmentation in (7) is given by

$$\mathbf{y} = \arg \min_{\mathbf{y} \in \mathcal{L}^o} \left\{ \sum_{j=1}^o -\log p(y_j | s_j) - \mu \sum_{j \sim k} \varphi(y_j - y_k) \right\}. \quad (9)$$

In this letter, we utilize the  $\alpha$ -expansion graph-cut-based algorithm [20], which yields a good approximation to the MAP segmentation, with practical computational complexity  $O(n)$  [10], to solve this combinatorial optimization problem. To sum up the main processes of the proposed method, the flowchart can be shown as in Fig. 1.

### III. EXPERIMENTS

Here, we investigate the effectiveness of the proposed algorithm with an IKONOS image and a WorldView-2 image. The classifiers of SVM with radial basis function (RBF) kernel and

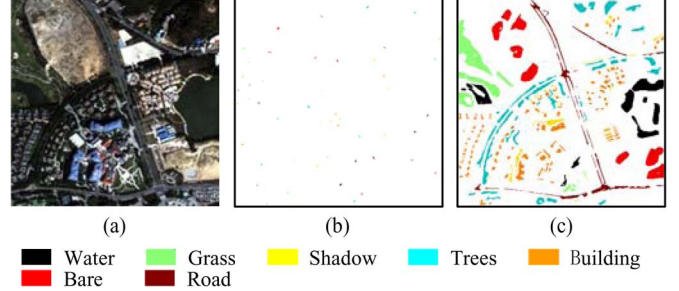


Fig. 2. Hainan data set. (a) True color image that takes bands 4, 3, and 2 as the red, green, and blue bands. (b) Training map. (c) Test map.

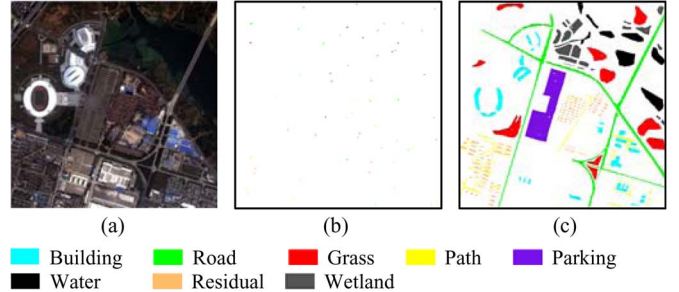


Fig. 3. Poyang data. (a) True color image that takes bands 1, 2, and 3 as the red, green, and blue bands. (b) Training map. (c) Test map.

TABLE II  
SEVEN GROUND TRUTH CLASSES IN THE WORLD VIEW-2 HAINAN DATA SET AND THE TRAINING AND TEST SAMPLE SETS FOR EACH CLASS

Class information	Number of training samples	Number of test samples
Water	39	3980
Grass	52	4927
Shadow	30	4028
Trees	37	1014
Building	32	3511
Bare	34	4286
Road	32	2539
Total	256	24258

TABLE III  
EIGHT GROUND-TRUTH CLASSES IN THE IKONOS POYANG DATA SET AND THE TRAINING AND TEST SAMPLE SETS FOR EACH CLASS

Information class	Number of training samples	Number of test samples
Building	18	3121
Road	28	5492
Grass	22	5341
Path	28	1526
Parking	20	4508
Residual	20	1454
Wetland	19	2997
Water	17	3480
Total	172	27919

SRC are used as the benchmarks in this letter. To evaluate the effectiveness of the combination of all the steps in the proposed algorithm, the classifiers are all shown in Table I. ‘‘S’’ in the second column stands for spectral feature, and ‘‘E’’ stands for EMAP feature; ‘‘PC’’ in the third column refers to pixel-based classification, ‘‘OOC’’ refers to object-oriented classification, and ‘‘Seg’’ refers to segmentation. All the segmentation steps in the experiments are implemented by graph cut. The parameters

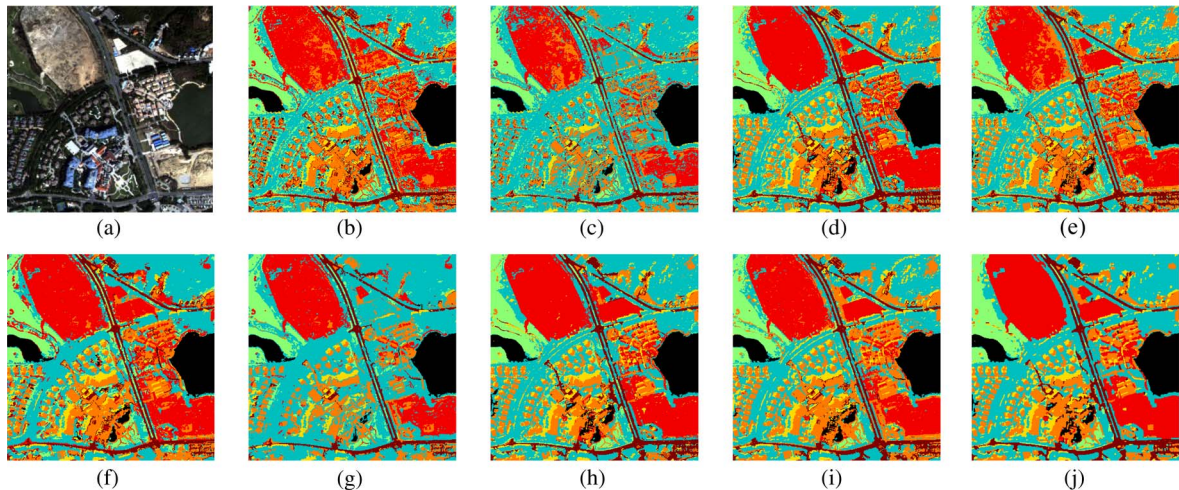


Fig. 4. Classification results with the Hainan image. (a) True color image that takes bands 4, 3, and 2 as the red, green, and blue bands. (b) SRC. (c) SVM. (d) SRC\_EAP. (e) SVM\_EAP. (f) OOSRC. (g) OOSVM. (h) OOSRC\_EAP. (i) OOSVM\_EAP. (j) Proposed.

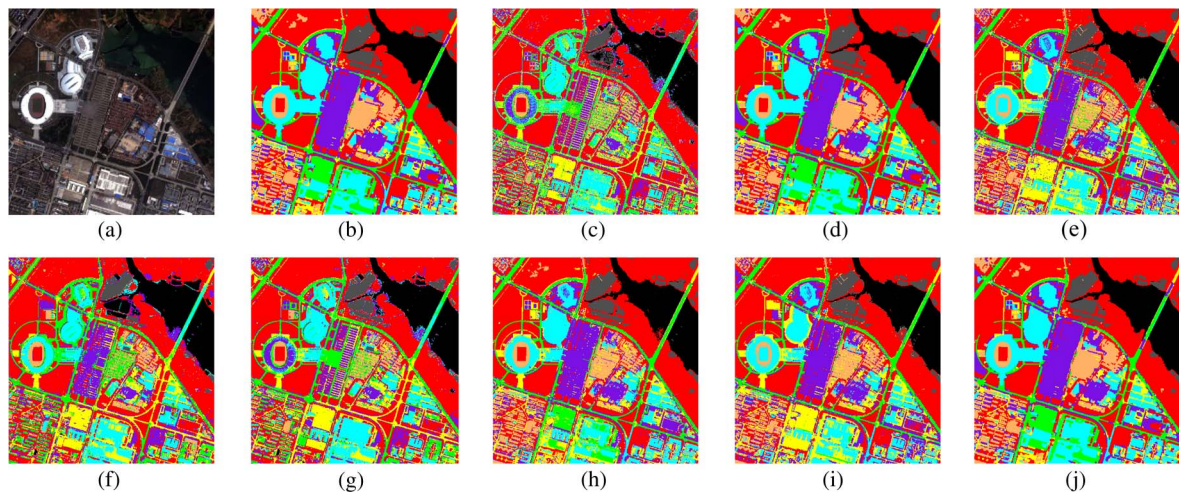


Fig. 5. Classification results with the Poyang image. (a) True color image that takes bands 4, 3, and 2 as the red, green, and blue bands. (b) SRC. (c) SVM. (d) SRC\_EAP. (e) SVM\_EAP. (f) OOSRC. (g) OOSVM. (h) OOSRC\_EAP. (i) OOSVM\_EAP. (j) Proposed.

associated with both the SVM- and SRC-based approaches are obtained by tenfold cross-validation.

The WorldView-2 and IKONOS imagery are of interest since they both provide rich spatial information (eight bands with 2.0-m spatial resolution for WorldView-2 and four bands with 4.0-m spatial resolution for IKONOS). The true colors of the WorldView-2 image and the IKONOS image are shown in Figs. 2(a) and 3(a), respectively. Figs. 2(b) and 3(b) show the training image of the Hainan data set and that of the Poyang data set, whereas Figs. 2(c) and 3(c) are the corresponding test images (both are rural areas with pixels). The test reference images were generated by field campaign and a visual interpretation of the study areas. The numbers of training and test samples for the WorldView-2 data set are shown in Table II, and those for the IKONOS data set are shown in Table III.

The challenge for the classification of the Hainan data set is to distinguish the spectrally similar classes such as soil–roads–roofs, trees–grass, and water–shadow. The smoothing parameter  $\mu$  for both images is set to 0.2, with regard to the high resolution, and the parameter associated with the sparse transform is also set as the optimal. The classification

maps of the various methods are shown in Fig. 4(b)–(j) for the WorldView-2 data set, and those for the IKONOS data set are shown in Fig. 5(b)–(j). The quantitative evaluation results, which include the classification accuracies for each class, the overall accuracy (OA), and the kappa coefficient ( $\kappa$ ), are shown in Tables IV and V, respectively. It can be seen that, for most classes, the four EMAP-feature-based classifiers outperform the ones with the spectral feature, and the proposed algorithm shows the best performance for both images. It can be seen in Figs. 4 and 5 that the proposed algorithm can produce an optimal visual map, which wipes out the “salt and pepper” misclassification phenomenon of the pixel-based algorithms, and can obtain more suitable segmentation regions than the object-oriented algorithms. To sum up, it is verified that the proposed method leads to a more effective and stable performance, when compared with these other widely used classifiers.

#### IV. CONCLUSION

This letter introduces a novel supervised segmentation method for VHR images by the use of EAPs and a sparse

TABLE IV  
CLASSIFICATION ACCURACIES FOR THE HAINAN DATA SET

CLASS	SRC	SVM	SRC_EAP	SVM_EAP	OOSRC	OOSVM	OOSRC_EAP	OOSVM_EAP	Proposed
1	0.9972	0.9955	<b>1</b>	<u>0.9997</u>	0.9987	0.9776	<b>1</b>	0.9995	<b>1</b>
2	0.8593	0.9319	0.9746	0.9642	0.9484	0.9850	0.9864	<u>0.9949</u>	<b>0.9955</b>
3	0.9950	0.9757	0.9916	0.9891	0.9995	0.9916	<u>0.9970</u>	0.9968	<b>0.9978</b>
4	0.9240	0.2039	0.9813	0.2499	0.9162	0.7594	<b>0.9832</b>	0.9734	<u>0.9822</u>
5	0.7867	0.2186	0.8411	0.2354	0.8396	0.7297	0.8584	<u>0.8698</u>	<b>0.8718</b>
6	0.8880	0.7299	<u>0.9930</u>	0.8663	0.9802	0.9669	0.9970	0.9839	<b>1</b>
7	0.9606	0.6453	<u>0.9925</u>	0.6903	0.9716	0.9709	0.9913	0.9866	<b>0.9965</b>
OA	0.9123	0.7288	0.9677	0.7679	0.9561	0.9339	0.9741	<u>0.9742</u>	<b>0.9791</b>
$\mathcal{K}$	0.8957	0.6818	0.9615	0.7292	0.9477	0.9209	0.9692	<u>0.9692</u>	<b>0.9751</b>

TABLE V  
CLASSIFICATION ACCURACIES FOR THE IKONOS POYANG DATA SET

CLASS	SRC	SVM	SRC_EAP	SVM_EAP	OOSRC	OOSVM	OOSRC_EAP	OOSVM_EAP	Proposed
1	0.8491	0.7504	0.9789	0.9766	0.9587	0.7337	<b>0.9878</b>	0.9667	<u>0.9837</u>
2	0.4252	0.4865	0.6072	0.6733	0.4860	0.5881	<b>0.7580</b>	<u>0.7238</u>	0.7200
3	0.9899	0.9946	<u>0.9996</u>	<b>1</b>	0.9910	0.9951	0.9994	<b>1</b>	<b>1</b>
4	0.5000	0.6088	0.6606	<b>0.6789</b>	0.6461	0.6691	0.6363	<u>0.6671</u>	0.5852
5	0.5976	0.5807	0.9352	0.9122	0.7578	0.5847	<u>0.9379</u>	0.9179	<b>0.9927</b>
6	0.5385	0.5048	0.8549	0.7565	0.4271	0.5103	<u>0.8549</u>	0.7758	<b>0.9188</b>
7	0.6880	0.7464	0.9983	<b>0.9993</b>	0.4468	0.9253	0.9970	<b>0.9993</b>	<u>0.9987</u>
8	0.9851	0.9845	<u>0.9997</u>	0.9991	0.9986	0.9963	0.9994	0.9974	<b>1</b>
OA	0.7164	0.7260	0.8835	0.8885	0.7447	0.7692	<u>0.9131</u>	0.8984	<b>0.9149</b>
$\mathcal{K}$	0.6704	0.6811	0.8639	0.8698	0.7025	0.7309	<u>0.8983</u>	0.8812	<b>0.9003</b>

transform. It is the first time that sparse representation has been utilized in VHR remote sensing imagery, by constructing the EMAP feature, which simultaneously preserves the spectral and the geometrical information. The MAP segmentation approach is also utilized in the proposed method, which integrates the class-dependent residuals by sparse representation and the MLL prior. A comparison of the proposed method with other state-of-the-art classifiers with data sets collected by the WorldView-2 and IKONOS sensors has confirmed the stable and competitive performance of the proposed method.

#### REFERENCES

- [1] M. Dalla Mura, J. Atli Benediktsson, B. Waske, and L. Bruzzone, "Morphological attribute profiles for the analysis of very high resolution images," *IEEE Trans. Geosci. Remote Sens.*, vol. 48, no. 10, pp. 3747–3762, Oct. 2010.
- [2] M. Dalla Mura, A. Villa, J. A. Benediktsson, J. Chanussot, and L. Bruzzone, "Classification of hyperspectral images by using extended morphological attribute profiles and independent component analysis," *IEEE Geosci. Remote Sens. Lett.*, vol. 8, no. 3, pp. 542–546, May 2011.
- [3] E. J. Candès, J. Romberg, and T. Tao, "Robust uncertainty principles: Exact signal reconstruction from highly incomplete frequency information," *IEEE Trans. Inf. Theory*, vol. 52, no. 2, pp. 489–509, Feb. 2006.
- [4] E. J. Candès and T. Tao, "Near-optimal signal recovery from random projections: Universal encoding strategies?" *IEEE Trans. Inf. Theory*, vol. 52, no. 12, pp. 5406–5425, Dec. 2006.
- [5] J. Wright, A. Y. Yang, A. Ganesh, S. S. Sastry, and Y. Ma, "Robust face recognition via sparse representation," *IEEE Trans. Pattern Anal. Mach. Intell.*, vol. 31, no. 2, pp. 210–227, Feb. 2009.
- [6] M. Aharon, M. Elad, and A. Bruckstein, "K-SVD: An algorithm for designing overcomplete dictionaries for sparse representation," *IEEE Trans. Signal Process.*, vol. 54, no. 11, pp. 4311–4322, Nov. 2006.
- [7] Y. Chen, N. M. Nasrabadi, and T. D. Tran, "Hyperspectral image classification using dictionary-based sparse representation," *IEEE Trans. Geosci. Remote Sens.*, vol. 49, no. 10, pp. 3973–3985, Oct. 2011.
- [8] H. Zhang, J. Li, Y. Huang, and L. Zhang, "A nonlocal weighted joint sparse representation classification method for hyperspectral imagery," *IEEE J. Sel. Topics Appl. Earth Observ. Remote Sens.*, 2013, doi: 10.1109/JSTARS.2013.2264720, to be published.
- [9] J. Li, H. Zhang, L. Zhang, and X. Huang, "Joint collaborative representation with multi-task learning for hyperspectral image classification," *IEEE Trans. Geosci. Remote Sens.*, vol. 52, no. 9, pp. 5923–5936, Sep. 2014.
- [10] Y. Boykov, O. Veksler, and R. Zabih, "Fast approximate energy minimization via graph cuts," *IEEE Trans. Pattern Anal. Mach. Intell.*, vol. 23, no. 11, pp. 1222–1239, Nov. 2001.
- [11] J. Li, J. M. Bioucas-Dias, and A. Plaza, "Spectral-spatial hyperspectral image segmentation using subspace multinomial logistic regression and Markov random fields," *IEEE Trans. Geosci. Remote Sens.*, vol. 50, no. 3, pp. 809–823, Mar. 2012.
- [12] M. Dalla Mura, J. Atli Benediktsson, B. Waske, and L. Bruzzone, "Extended profiles with morphological attribute filters for the analysis of hyperspectral data," *Int. J. Remote Sens.*, vol. 31, no. 22, pp. 5975–5991, Dec. 2010.
- [13] E. J. Breen and R. Jones, "Attribute openings, thinnings, and granulometries," *Comput. Vis. Image Underst.*, vol. 64, no. 3, pp. 377–389, Nov. 1996.
- [14] B. Song, J. Li, M. Dalla-Mura, P. Li, A. Plaza, J. M. Bioucas-Dias, J. A. Benediktsson, and J. Chanussot, "Remotely sensed image classification using sparse representations of morphological attribute profiles," *IEEE Trans. Geosci. Remote Sens.*, vol. 52, no. 8, pp. 5122–5136, Aug. 2014.
- [15] P. R. Marpu, M. Pedernana, M. Mura, J. A. Benediktsson, and L. Bruzzone, "Automatic generation of standard deviation attribute profiles for spectral-spatial classification of remote sensing data," *IEEE Geosci. Remote Sens. Lett.*, vol. 10, no. 2, pp. 293–297, Mar. 2013.
- [16] J. Li, H. Zhang, Y. Huang, and L. Zhang, "Hyperspectral image classification by nonlocal joint collaborative representation with a locally adaptive dictionary," *IEEE Trans. Geosci. Remote Sens.*, vol. 52, no. 6, pp. 3707–3719, Jun. 2014.
- [17] M. Elad, *Sparse and Redundant Representations: From Theory to Applications in Signal and Image Processing*. New York, NY, USA: Springer-Verlag, 2010.
- [18] D. L. Donoho and Y. Tsaig, *Fast Solution of  $l_1$ -Norm Minimization Problems When the Solution May Be Sparse*. Stanford, CA, USA: Dept. Stat., Stanford Univ., 2006.
- [19] J. Li, J. M. Bioucas-Dias, and A. Plaza, "Semisupervised hyperspectral image segmentation using multinomial logistic regression with active learning," *IEEE Trans. Geosci. Remote Sens.*, vol. 48, no. 11, pp. 4085–4098, Nov. 2010.
- [20] V. Kolmogorov and R. Zabih, "What energy functions can be minimized via graph cuts?" *IEEE Trans. Pattern Anal. Mach. Intell.*, vol. 26, no. 2, pp. 147–159, Feb. 2004.